$\Delta G(x,\mu^2)$ from jet and prompt photon production at RHIC

O. Martin and A. Schäfer
Institut für Theoretische Physik, Universität Regensburg, D-93040 Regensburg, Germany
(February 1, 2008)

We compare theoretical results for jet and prompt photon production in $\vec{p}\vec{p}$-collisions at RHIC obained with three different methods: a) the unpolarized event generator PYTHIA combined with hadronic asymmetry weights calculated from leading order formulae, b) the polarized event generator SPHINX which treats the partonic helicity in the hard scattering and the initial state shower explicitly, and c) parton generators which integrate next-to-leading order QCD cross sections using Monte Carlo methods. Method a) requires far less computer time than method b) but we find that it is too imprecise for precision studies. The lacking treatment of partonic polarization in the initial state shower results in relative deviations in the asymmetries of up to 20% relative to SPHINX (method b)). As was to be expected, the event generator predictions for the absolute cross sections differ significantly from the next-to-leading order QCD calculations. But fortunately the asymmetries show a much better agreement: relative deviations for prompt photon production for parameterizations with medium and large $\Delta g(x,\mu^2)$ barely exceed 10%. After fine tuning the parameters of the parton showers the same result can be obtained for jet production.

I. INTRODUCTION

One of the most remarkable features of high-energy hadron collisions is certainly their complexity. Particle multiplicities in single events are frequently of the order $\mathcal{O}(10^2\text{-}10^3)$ and will continue to rise with the advent of new colliders like BNL-RHIC and CERN-LHC. On the other hand, perturbative QCD (pQCD) can only deal with a limited number of final-state partons so that we have to ask, how these are related to experimentally measured distributions of hadrons and leptons. This is where event generators (EGs) come to the rescue.

Heavy use of EGs is made during the whole life cycle of a high energy physics experiment for purposes such as estimating absolute production rates, studying the background-to-signal ratio, studying the detector acceptance, testing the reliability of event reconstruction during experimental analysis, etc. For collisions of polarized hadrons this list must be extended to also include studying the size of the hadronic double spin asymmetries of the signal and the background, determining the sensitivity to the polarized parton distribution which is to be measured, calculating the *polarized acceptance*, etc. The last point is especially important for fragmented detector systems with a small geometrical coverage like PHENIX at RHIC (see, e.g., [1]). EGs for the simulation of collisions of longitudinally polarized particles must therefore include a correct treatment of particle helicity.

In order to see how this goal can be achieved let us summarize the principle of current EGs. The generation process is subdivided into several steps where the first one deals with the hard partonic scattering. For nucleon-nucleon scattering, parton flavours and kinematics are selected according to the factorization formula for the unpolarized cross section,

$$\mathrm{d}\sigma^{(AB)}(P_A;P_B)=\sum_{a,b}\int \mathrm{d}x_A\mathrm{d}x_B f_a^A(x_A,\mu^2)f_b^B(x_B,\mu^2)\mathrm{d}\hat{\sigma}_{a,b}(x_AP_A,x_BP_B,\mu)\,. \tag{1}$$

A, B (a, b) are the involved hadrons (partons), μ denotes the factorization and renormalization scale and the partonic cross section $\mathrm{d}\hat{\sigma}_{a,b}$ is evaluated to leading order (LO) in the strong coupling $\alpha_s(\mu)$. Please note, that the momenta of the colliding partons are so far parallel to the momenta of the colliding beams. Of course this picture is very simplified and is significantly altered by radiative corrections which are specific to every hard partonic reaction. However, certain parts of these radiative corrections, consisting of the collinear poles of each parton splitting, are universal and can be used to formulate a parton shower (PS) algorithm which can be applied to every partonic subprocess [2]. In this way an approximation of the complete perturbative series is obtained which becomes exact in the limit of vanishing decay angles and fails for large angles. The parton showers can be somewhat arbitrarily subdivided into an initial state shower (ISS) and a final state shower (FSS). The former generates all particles which directly 'connect' the two initial colliding partons with the ones that finally participate in the hard partonic reaction. It mimics the DGLAP evolution of parton densities in normal perturbative calculations but there is also an important difference: each parton branching also involves transverse momentum which in general leads to a Lorentz boost and rotation of the partonic

scattering system. Thus, the ISS changes the kinematics of the partons (for details see [2]). Finally, the numerous partons produced by the PS fragment into stable and unstable hadrons which are then allowed to decay. Thus, EGs provide complete events which are in principle as detailed as real events that could be measured with a perfect detector. In an ideal case, they would also show the same fluctuation properties.

An approximate treatment of polarization can be achieved relatively easy and has so far been used by the members of the RHIC Spin Program [3] to prepare the experiments [4]:

- Generate unpolarized events with the unpolarized EG PYTHIA [5]. Extract the kinematics (x_A, x_B, $\hat{s}$, $\hat{t}$, $\hat{u}$, μ) and the flavours of the hard partonic interaction. The partonic Mandelstam variables follow the usual definitions

$$\hat{s} = (x_A P_A + x_B P_B)^2\,, \quad \hat{t} = (x_A P_A - k_1)^2\,, \text{ and } \quad \hat{u} = (x_A P_A - k_2)^2\,, \tag{2}$$

  where $k^\mu_{1,2}$ are the momenta of the outgoing partons.

- For each observable plot two histograms. The first histogram with the weight set to 1 gives the unpolarized cross section. For the second one the weight is taken to be the hadronic double spin asymmetry

$$A_{LL}^{(AB)}(x_A, x_B, \hat{s}, \hat{t}, \hat{u}, \mu^2) = \frac{\Delta f_a^A(x_A,\mu)}{f_a^A(x_A,\mu)} \frac{\Delta f_b^B(x_B,\mu)}{f_b^B(x_B,\mu)} \frac{\Delta\hat{\sigma}_{a,b}(\hat{s},\hat{t},\hat{u},\mu^2)}{\hat{\sigma}_{a,b}(\hat{s},\hat{t},\hat{u},\mu^2)}\,. \tag{3}$$

  The formulae for the partonic double spin asymmetries $\Delta\hat{\sigma}_{a,b}/\hat{\sigma}_{a,b}$ for the processes relevant for this work can be found in Table I.

PYTHIA process number	partonic reaction	partonic asymmetry $\frac{\Delta\hat{\sigma}}{\hat{\sigma}}$	remark
11	$qq' \to qq'$	$\left(\hat{s}^2-\hat{u}^2\right) / \left(\hat{s}^2+\hat{u}^2\right)$	
	$q\bar{q}' \to q\bar{q}'$	$\left(\hat{s}^2-\hat{u}^2\right) / \left(\hat{s}^2+\hat{u}^2\right)$	
	$q\bar{q} \to q\bar{q}$	$\left[\hat{s}\left(\hat{s}^2-\hat{u}^2\right)+\frac{2}{3}\mathcal{I}\hat{t}\hat{u}^2/\mathcal{K}\right] / \left[\hat{s}\left(\hat{s}^2+\hat{u}^2\right)-\frac{2}{3}\mathcal{I}\hat{t}\hat{u}^2/\mathcal{K}\right]$	$\hat{t}$- and $\hat{u}$-channel only
	$qq \to qq$	$\left(\hat{s}^2-\hat{u}^2\right) / \left(\hat{s}^2+\hat{u}^2\right)$	colour flow scenario 1
		$\left[\hat{t}\left(\hat{s}^2-\hat{t}^2\right)-\frac{2}{3}\mathcal{I}\hat{s}^2\hat{u}\right] / \left[\hat{t}\left(\hat{s}^2+\hat{t}^2\right)-\frac{2}{3}\mathcal{I}\hat{s}^2\hat{u}\right]$	colour flow scenario 2
12	$q\bar{q} \to q\bar{q}$	-1	$\hat{s}$-channel only
	$q\bar{q} \to q'\bar{q}'$	-1	
13	$q\bar{q} \to gg$	-1	
14	$q\bar{q} \to g\gamma$	-1	
18	$q\bar{q} \to \gamma\gamma$	-1	
28	$qg \to qg$	-1	colour flow scenario 1
		1	colour flow scenario 2
29	$qg \to q\gamma$	$\left(\hat{s}^2-\hat{u}^2\right) / \left(\hat{s}^2+\hat{u}^2\right)$	
53	$gg \to q\bar{q}$	-1	
68	$gg \to gg$	$-\left[\hat{t}^2+2\hat{s}\hat{t}\left(\hat{s}^2+\hat{t}^2\right)+3\hat{s}^2\hat{t}^2\right] / \left[\hat{s}^2+\hat{t}^2+2\hat{s}\hat{t}\left(\hat{s}^2+\hat{t}^2\right)+3\hat{s}^2\hat{t}^2\right]$	colour flow scenario 1
		$-\left[\hat{u}^2+2\hat{s}\hat{u}\left(\hat{s}^2+\hat{u}^2\right)+3\hat{s}^2\hat{u}^2\right] / \left[\hat{s}^2+\hat{u}^2+2\hat{s}\hat{u}\left(\hat{s}^2+\hat{u}^2\right)+3\hat{s}^2\hat{u}^2\right]$	colour flow scenario 2
		$2\left[\hat{t}\hat{u}\left(\hat{t}^2+\hat{u}^2\right)+3\hat{t}^2\hat{u}^2\right] / \left[\hat{t}^2+\hat{u}^2+2\hat{t}\hat{u}\left(\hat{t}^2+\hat{u}^2\right)+3\hat{t}^2\hat{u}^2\right]$	colour flow scenario 3

TABLE I. Partonic double spin asymmetries of all LO processes relevant to the production of QCD jets and prompt photons. The enumeration of color flow scenarios follows the values of the internal PYTHIA variable `MINT(2)` [6]. $\mathcal{I} = 1$, if the color interference terms are to be included, otherwise $\mathcal{I} = 0$. $\mathcal{K}$ is a K-factor with the default value $\mathcal{K} = 1$.

- After the event generation is completed, divide the second histogram by the first one to obtain the hadronic double spin asymmetry. Finally, normalize the first histogram appropriately.

We shall call this prescription the method of asymmetry weights (MAW) in the remainder of this paper. It is clearly only an approximation to the 'true answer' within the EG model because it does not describe how parton showers depend on the parton helicities.

A simple way to overcome this deficit was presented by the authors of the EG SPHINX [7] which is a polarized version of PYTHIA. It uses hadronic and partonic cross sections which depend on the helicities of the incoming hadrons $H_{A,B}$ and partons $h_{a,b}$ and which are summed over the polarization of the outgoing particles. The kinematics of the partonic reaction is therefore generated according to

$$\mathrm{d}\sigma^{(AB)}(P_A,H_A;P_B,H_B)=\sum_{a,h_a,b,h_b}\int \mathrm{d}x_A\mathrm{d}x_B f^{A,H_A}_{a,h_a}(x_A,\mu^2)f^{B,H_B}_{b,h_b}(x_B,\mu^2)\mathrm{d}\hat{\sigma}_{ah_a,bh_b}(x_AP_A,x_BP_B,\mu^2)\,, \tag{4}$$

$$f^{A,H_A}_{a,h_a}(x_A,\mu^2)=\frac{1}{2}\left[f^A_a(x_A,\mu^2)+\delta_{\epsilon(H_A),\epsilon(h_a)}\Delta f^A_a(x_A,\mu^2)-\delta_{\epsilon(H_A),-\epsilon(h_a)}\Delta f^A_a(x_A,\mu^2)\right]\,, \tag{5}$$

where $\epsilon(x)$ is the sign function [8]. Similarly, the helicity of all partons participating in the ISS is chosen according to the helicity dependent DGLAP splitting functions

$$P_{bh_b,ah_a}(z)=\frac{1}{2}\left[P_{ba}(z)+\delta_{\epsilon(h_b),\epsilon(h_a)}\Delta P_{ba}(z)-\delta_{\epsilon(h_b),-\epsilon(h_a)}\Delta P_{ba}(z)\right] \tag{6}$$

instead of using the usual unpolarized $P_{ba}(z)$ as in PYTHIA. Following this procedure one directly gets the cross sections for different helicity configurations of the colliding hadrons. They can be combined according to

$$A^{(AB)}_{LL}=\frac{\mathrm{d}\sigma^{(AB)}(P_A,+;P_B,+)-\mathrm{d}\sigma^{(AB)}(P_A,+;P_B,-)}{\mathrm{d}\sigma^{(AB)}(P_A,-;P_B,+)+\mathrm{d}\sigma^{(AB)}(P_A,+;P_B,-)} \tag{7}$$

to obtain the hadronic double spin asymmetry. It is clear, that one needs events as generated by SPHINX to test the experimental analysis software. SPHINX has, however, a severe disadvantage in comparison to the MAW. Longitudinal double spin asymmetries in $\vec{p}\vec{p}$-collisions are frequently of the order of 1% which means that 10^6 *accepted* events per bin are necessary to achieve a relative statistical Monte Carlo (MC) error of 10%. The MAW needs much less computation time since it calculates the asymmetry directly and not by computing the relative difference between two similarly large numbers. Furthermore, it allows for the simultaneous usage of multiple parameterizations of polarized parton distributions because they are irrelevant for the generation of the event itself. Depending on the size of the asymmetry computation times easily differ by a factor of the order $\mathcal{O}(10^2)$. However, this speed advantage is useless if both methods yield largely different results for the hadronic double spin asymmetries. So far, no systematic comparison using realistic experimental cuts for the relevant observables has been performed for the RHIC Spin Project or any other experiment according to the authors' knowledge. Since this question is so important we have done the necessary simulations and present our results in this paper.

We would also like to stress that rates and asymmetries calculated with SPHINX should not be regarded as the ultimate truth. EGs possess some serious shortcomings which their users should always be aware of. The foremost problem stems from the fact that LO expressions for the cross sections and splitting functions are used throughout. The resulting large scale dependences prohibit reliable predictions of absolute cross sections or rates. Changes in some of the numerous necessary parameters of the PS model also may have quite strong effects on counting rates. Being aware of this issue we should try to clarify if the polarized EGs nevertheless yield a good description of nature. Unfortunately, this is currently impossible because so far no $\vec{p}\vec{p}$-collisions have been studied. We can only compare with the unpolarized results for the wide range of available pp- and $p\bar{p}$-data but even this task is non-trivial without access to the analysis software of the various collaborations.

Since we are more interested in the polarized sector anyway, we decided to rather study the uncertainty of theoretical predictions by comparing the EG results with next-to-leading order (NLO) QCD calculations. In some sense, both methods are complementary because they take different parts of the perturbative series into account. Furthermore, NLO predictions depend on a minimal set of parameters which includes only the intrinsic QCD scale Λ_{QCD}, the renormalization, factorization and in some cases the fragmentation scales. Usually this dependence is much smaller than in LO calculations effectively giving NLO QCD predictive power with regards to absolute rates. In some cases, agreement with experiment has been quite spectacular. E.g., the NLO calculation of the transverse energy spectrum of inclusive 1-jet production at TEVATRON at $\sqrt{S}=1.8$ GeV agrees very well with data even though the unpolarized cross section varies over a range of six orders in magnitude [9]. Unfortunately, NLO calculations tend to get unrealiable if highly restrictive experimental acceptances are involved. We assume that NLO QCD will also do a good job for

polarized jet production at RHIC which was shown to be very sensitive to the polarized gluon distribution $\Delta g(x,\mu^2)$ [10], the prime target of most measurements at RHIC and take the differences when compared to EG results as estimate for the theoretical systematic error. Originally, prompt photon production has been promoted as the most useful process for the measurement of $\Delta g(x,\mu^2)$ but currently the situation in the unpolarized sector is far from satisfactory. Aside from the fact that NLO QCD cannot fit all available data sets with one set of scales in the fixed-target energy range, there also seem to be inconsistencies between some data sets [11]. Under very lucky circumstances these problems may happen to cancel when taking ratios of polarized and unpolarized cross sections but of course we should not count on it. Whatever the solution to the current problems will be, NLO QCD will always be an integral part of it. For this reason, we also decided to not only compare jet observables but to also undertake a systematic comparison of prompt photon observables calculated with EGs and NLO QCD. For this purpose we use the parton generators of [10,12] which use MC techniques to integrate NLO cross sections and permit the implementation of simple cuts on the final state.

After discussing the necessary technical preliminaries we will present our results for jet observables in section 2 whereas section 3 will deal with prompt photon production only. The final section summarizes our findings and contains the conclusions.

II. PRODUCTION OF QCD-JETS

The authors of Ref. [10] have already studied 1-jet and 2-jet observables in longitudinally polarized $\vec{p}\vec{p}$-collisions at the maximal RHIC cm-energy of $\sqrt{S} = 500$ GeV using their NLO QCD parton generator. STAR is the only available detector system at RHIC which is able to perform such measurements. After installation of the endcap its acceptance region will cover $-1 < \eta < 2$ in pseudorapidity and $0 < \phi < 2\pi$ in azimuthal angle. The main results of [10] are that the perturbative series of the polarized cross section is under control, that parameterizations with different $\Delta g(x,\mu^2)$ yield very distinctive asymmetries and that the statistical experimental error will be sufficiently small to allow for a precise measurement from which the polarized gluon distribution can be determined. Therefore, [10] is an ideal basis for our studies and we can use the same observables without any worries about perturbative stability.

Before we give a detailed description of them let us make a few remarks on the choice of the parton distributions and the QCD running coupling constant. Nowadays, polarized inclusive lepton-nucleon scattering still has the by far largest impact on the determination of the polarized parton distributions. Unfortunately, the current data are not precise enough and cover a too small x-Q^2-range to give any useful restriction on $\Delta g(x,\mu^2)$. As a consequence, LO and NLO fits based on the same assumptions and restrictions may give widely different results for the polarized gluon distribution, i.e. the ratio

$$K_{\Delta g}(x,\mu^2) = \frac{\Delta g^{\mathrm{NLO}}(x,\mu^2)}{\Delta g^{\mathrm{LO}}(x,\mu^2)} \tag{8}$$

can deviate strongly from 1. According to Fig. 1 this is indeed the case for two of the three sets of polarized parton distributions we use in our studies. Although the EGs are only based on LO QCD we would therefore be ill advised to use them in combination with LO parton distributions. Any agreement with NLO QCD results would be purely accidental, especially in view of the sensitivity of jet production towards $\Delta g(x,\mu^2)$. Accordingly, we also use the NLO expression for the strong coupling $\alpha_s(\mu^2)$ throughout to ensure that the EG without PS and the lowest order perturbative calculation will give the same results. The unpolarized GRV [13] as well as the polarized GRSV [14] and DSS [15] parameterizations we use are already quite old. Nevertheless, they still fulfill all our needs since we are interested in comparing different methods of calculation rather than making precise predictions. It is more important here to ensure that for each polarized set we use the correct unpolarized set of distributions which in all cases is GRV. Otherwise SPHINX will not give correct results because it makes use of the unpolarized and polarized set simultaneously, so that only one value can be given for Λ_{QCD}. The three selected sets of $\Delta f(x,\mu^2)$ pretty much cover the whole range of possible values for $\Delta g(x,\mu^2)$ with GRSV $g_{\max}$ giving the largest and DSS3 the smallest values. In all cases the scales were set equal to the average transverse momentum of the partons leaving the hard partonic interaction:

$$\mu = \frac{1}{n}\sum_{i=1}^{n} |k_{T,i}| \,. \tag{9}$$

A. The observables

We already mentioned that the number of final-state partons is much larger in the EG model than in perturbative calculations even though both intend to describe the same physics. For our studies we should therefore pick a jet-clustering algorithm which depends only weakly on particle multiplicities. The Ellis-Soper k_T-algorithm [16] with the preferred choice of $R = 1$ suits our needs. For each event it gives the number of reconstructed jets as well as their transverse energies E_T, pseudorapidities η and azimuthal direction ϕ. From these we construct four observables[1] which are defined as follows:

- the E_T-dependent 1-jet inclusive cross section $\mathrm{d}(\Delta)\sigma/\mathrm{d}E_T$, 14 GeV$< E_T <$ 50 GeV;
- the η-dependent 1-jet inclusive cross section $\mathrm{d}(\Delta)\sigma/\mathrm{d}\eta$, $0 < \eta < 2$, $E_T > 15$ GeV. Since the cross section is symmetric in η we restrict ourselves to the region of positive pseudorapidity.

For all 2-jet inclusive observables we denote the hardest and second hardest jet by J_1 and J_2 and demand

$$E_{T,J_1} > 15 \text{ GeV}\,, \quad E_{T,J_2} > 10 \text{ GeV}\,, \quad |\eta_{J_1}| < 1\,, \quad |\eta_{J_2}| < 1\,. \tag{10}$$

The asymmetric cut on the transverse energies reduces contributions from configurations in which the two leading jets are exactly back-to-back and which cannot be calculated with finite order perturbation theory [10]. All events fulfilling the requirement (10) are considered for

- the distribution of the rapidity difference $\mathrm{d}(\Delta)\sigma/\mathrm{d}\Delta\eta\,,\ 0 < \Delta\eta < 2\,,\ \Delta\eta = \eta_{J_1} - \eta_{J_2}\,;$
- the distribution of the invariant jet mass M_{JJ} defined by $\mathrm{d}(\Delta)\sigma/\mathrm{d}M_{JJ}\,,\ M_{JJ} < 100$ GeV, $M_{JJ}^2 = (p_{J_1} + p_{J_2})^2$.

B. Comparison of the EG methods

Event generators are very complex programs which often consist of several ten thousand lines of code and are equipped with a large number of options. In order to avoid errors we should try to reuse as much program code as possible for our comparisons of EG methods and NLO calculations. This can be easily achieved, because SPHINX can also be operated in an unpolarized mode, in which it corresponds to PYTHIA 5.6 and only needs to be extended with a function that calculates the asymmetry weights of Table I. Furthermore, the EG and the NLO parton generators use the same code to evaluate the parton distributions and the strong coupling constant.

The absolute statistical MC error of the asymmetries calculated with SPHINX is only determined by the number of accepted events in a certain bin and is therefore independent of the actual size of the asymmetries. In order to maximize the precision and reduce the required computer time we should use parton densities which yield large asymmetries, i.e. GRSV $g_{\max}$ is the preferred set. The artifical set $\Delta f(x,\mu^2) = f(x,\mu^2)$ generally yields even larger asymmetries but cannot be used within the PS model since it is inconsistent with DGLAP evolution. By running SPHINX and PYTHIA with PS switched *off*, we made sure that the implementation of the asymmetry weights is indeed correct. The relative deviations between asymmetries calculated with SPHINX and the MAW did not exceed 2% and were within the statistical MC accuracy. We want to stress, that during all EG runs the hadronization and intrinsic partonic transverse momentum were switched off so that the results can be better compared to NLO calculations.

Fig. 2 shows the results for the (un)polarized cross sections, asymmetries and the relative deviations

$$R_\sigma = \frac{\mathrm{d}\sigma_{\text{MAW}} - \mathrm{d}\sigma_{\text{SPHINX}}}{\mathrm{d}\sigma_{\text{MAW}}}\,, \quad R_A = \frac{A_{LL,\text{MAW}} - A_{LL,\text{SPHINX}}}{A_{LL,\text{MAW}}} \tag{11}$$

between the MAW ($8 \cdot 10^6$ generated events) and SPHINX ($4 \cdot 10^7$ generated events) with the PS switched *on*. Let us concentrate on the right column, in which the full black line represents R_σ. In all cases it is either compatible with or very close to zero so that we proved once more that the spin averaging of SPHINX indeed works. The dashed crosses represent R_A calculated with *polarized treatment switched on* in the ISS of SPHINX. For all four observables systematic deviations show up. The asymmetries for the two 1-jet observables calculated with the MAW are generally about 5% larger than the ones which are calculated with SPHINX. The differences are especially strong in the large η-region,

[1] We actually studied more observables but they did not yield any new insights.

where they reach 20%. However, these findings cannot be generalized to all observables. For the $\Delta\eta$-distributions and the region of small invariant mass the situation is reversed. Within the limited accumulated MC statistics, both methods seem to yield the same asymmetries for large M_{JJ} but even here we can note a tendency for systematic differences towards positive R_A. In order to pin down the origin of the large deviations we also carried out an analysis of events generated by SPHINX for which the *polarized treatment in the ISS was switched off* (dotted crosses in Fig. 2). From the fact, that $R_A(\eta)$ is now compatible with zero for large pseudorapidity we conclude, that the largest part of the deviations is indeed caused by the missing treatment of parton helicity within the MAW approach. However this cannot be the full story because R_A is not compatible with zero for all other observables. But keeping in mind that the ISS changes the kinematics of the hard partonic interaction, that within the MAW the ISS is applied to unpolarized events whereas within SPHINX it is applied to polarized events with different configurations of proton helicities, it is clear that the ISS can slightly modify the asymmetry even though polarized treatment is switched off. Unfortunately we were unable to check if the same results also hold true for the two other sets of polarized parton distributions. As we will see in Fig. 4, the set GRSV std. (DSS3) yields asymmetries which are smaller by a factor of five (twenty) so that we would have had to generate $1 \cdot 10^9$ ($1.6 \cdot 10^{10}$) events with SPHINX to obtain the same relative statistical accuracy. This was simply beyond the means of our computer equipment.

C. Comparison of the MAW with NLO QCD predictions

In view of the fact that parton helicity plays a significant role in the ISS we would have liked to compare SPHINX with NLO QCD. Unfortunately, this was impossible for the same exact reasons as were given at the end of the previous paragraph. We resort to comparing the results of the MAW with NLO QCD predictions so that several different parameterizations of polarized parton densities can be used.

In order to find a common basis we again start out by comparing Born-results, i.e. observables calculated with LO partonic cross sections, NLO parton distribution, and a NLO expression for the running strong coupling. For this purpose, Fig. 3 shows the relative deviations of the unpolarized cross sections and the asymmetries defined by

$$R_\sigma \equiv \frac{\mathrm{d}\sigma_{\text{(N)LO QCD}} - \mathrm{d}\sigma_{\text{MAW}}}{\mathrm{d}\sigma_{\text{(N)LO QCD}}}\,, \quad R_A \equiv \frac{A_{LL,\text{(N)LO QCD}} - A_{LL,\text{MAW}}}{A_{LL,\text{(N)LO QCD}}}\,. \tag{12}$$

Only the error bars of R_σ are plotted for the sake of clarity, as the error bars of R_A can be estimated from the statistical fluctuation between two neighbouring bins. The unpolarized cross sections and the asymmetries for both GRSV sets mainly show a satisfactory, but not perfect agreement for the bins with high statistics. This is unfortunately not the case for the DSS3 set – even for bins with good statistics deviations of 5% show up although both programs use the same routines to evaluate the parton distributions, as was already mentioned before. The reason for these problems is still under investigation but we assume, that it is most likely caused by the different treatment of colour interference terms (c.f. [6]) and the fact, that the relatively small asymmetries of the large number of contributing partonic processes undergo a delicate cancellation process. We will soon see that PS or NLO corrections to the asymmetries will be by far stronger so that we can effectively neglect the just mentioned problems.

PYTHIA parameter	description	default value	optimized value
`PARP(64)`	argument of α_s for each parton splitting divided by $k_\perp^2$	1	2.5
`PARP(65)`	minimal energy of an emitted parton	2 GeV	3 GeV
`PARP(67)`	maximal scale of the ISS divided by μ	4	3

TABLE II. Modified parameters of the ISS which were used for the calculations of Fig. 5.

In an ideal case, the results of NLO QCD and the MAW would just agree. This is of course very unlikely. Just by considering the scale dependence of the observables, which is much larger for the EG, we see that agreement can only be achieved for one special scale or even not at all, because the results might not only differ in their normalization but also in their shape. So it is not surprising, that the cross sections calculated with both methods deviate by up to 40% when using the standard choice of scales and the standard PS parameters (see Fig 4). However, the objects we are mainly interested in, namely the asymmetries, show a much better agreement. R_A seldomly exceeds 20% for any of the three polarized sets and the agreement is about twice as 'good' for $A_{LL}(M_{JJ})$.

The PS needs a number of parameters which can be freely varied within certain limits and have to be determined by fitting to data. We picked three of of them, listed in Table II, and tried to refit them using the NLO QCD calculation as 'data set'. Due to the long necessary computation time an automated fitting procedure is unpractical and we resort to manually testing a few values. The E_T- and η-dependent observables are the most inclusive ones so that their normalization should be fixed first, aside from improving the agreement of the asymmetries. Accordingly, the absolute rates predicted by the EG have to be reduced which can be achieved by reducing the activity of the ISS. Table II shows the default as well as the fitted values of the three parameters. Since the fitting was done manually with a very limited number of different values it is unlikely that the optimal set has been found. Nevertheless, a look at Fig. 5 shows that it completely fulfills its purpose: the unpolarized cross sections for the 1-jet inclusive observables as well as the asymmetries for the two GRSV sets now agree at a 10% level whereas the situation for the set DSS3 is not quite as good. On the other hand, the agreement for the 2-jet inclusive rates got much worse.

In order to get a feeling for the size of the relative deviations we study the scale dependence of the NLO predictions. In Fig. 6 the standard choice of the scales (9) is varied by a factor of 0.5 and 2, resp., which results in the bands of cross section displayed in the left column of the figure. By dividing the minimal (maximal) polarized cross section by the maximal (minimal) unpolarized cross section we obtain the limits on the bands of asymmetries, which are shown in the right column. According to the figure, the optimized EG asymmetries are always within the bands. Aside from the normalization of the 2-jet inclusive cross sections, the EG results are therefore compatible with NLO QCD.

III. PROMPT PHOTON PRODUCTION

Let us now turn to the production of prompt photons in $\vec{p}\vec{p}$-collisions. This process receives a lot of interest mainly due to fact that the quark-gluon fusion $qg \to q\gamma$ strongly dominates at LO for medium sized and large $\Delta g(x, \mu^2)$. Before the trouble with the fixed-target data emerged, the analysis therefore seemed to be especially easy and clean. At the large cm-energies accessible at RHIC another problem arises: the majority of photons are actually not produced in the hard partonic interaction but through pion-decay into two photons. These fragmentation photons can luckily be completely filtered out by an isolation prescription defined in Ref. [17]. Unless the usual cone-isolation prescription, which limits the hadronic energy contained in a cone drawn around the photon direction in η-ϕ-space with opening angle δ_0, Frixione's prescription allows less hadronic energy the closer the hadrons are to the photon and no hadronic energy for exactly parallel hadrons. Since fragmentation is an exactly collinear process in QCD, this prescription effectively eliminates all fragmentation photons while at the same time the cancellation of soft and collinear divergences stays untouched. For our studies we choose $\delta_0 = 0.7$.

A. The observables

Common experience with polarized prompt photon calculations shows that asymmetries tend to become smaller when the cm-energy of the experiment is increased because smaller x-values are probed. For our event generator studies we therefore choose $\sqrt{S} = 200$ GeV instead of the maximal RHIC cm-energy which is beneficial for the precision of all results calculated with SPHINX. Our choice of observables follows closely the NLO QCD study of Ref. [12] for the same reasons that were given in section II. The cuts were inspired by the geometrical coverage of STAR. Frixione's isolation criterion in combination with the ES jet algorithm yields the transverse momentum, rapidity and azimuthal angle of the photon and a certain number of jets for all events which pass the isolation cut. These are then used to calculate two inclusive observables:

- the $p_{T,\gamma}$-dependent cross section $\mathrm{d}(\Delta)\sigma/\mathrm{d}p_{T,\gamma}$, 10 GeV$< p_{T,\gamma} <$50 GeV, $|\eta_\gamma| < 0.5$;
- the η_γ-dependent cross section $\mathrm{d}(\Delta)\sigma/\mathrm{d}\eta_\gamma$, $0 < \eta_\gamma < 2$, $p_{T,\gamma} > 10$ GeV. Due to symmetry we again restrict ourselves to the positive η-region.

Inclusive prompt photon observables have the advantage that counting rates are quite large. On the other hand, the kinematics of the hard partonic reaction can of course not be reconstructed. Thus, there is no one-to-one

correspondence between the measured transverse momentum of the photon and the probed gluonic x even in a LO analysis. This problem can be fixed if only events with one reconstructed jet are considered. Additionally, we require

$$p_{T,\gamma} > 10 \text{ GeV}\,, \quad E_{T,J} > 11 \text{ GeV}\,, \quad -1 < \eta_{\gamma,J} < 2\,, \quad |\Delta\phi| = |\phi_J - \phi_\gamma| > \frac{\pi}{2} \tag{13}$$

which effectively means that the jet must be located in the hemisphere opposite to the photon. Events with multiple jets are not considered here. Their simulation would require a NLO parton generator with so far unknown matrix elements of order $\mathcal{O}(\alpha\alpha_s^3)$ or higher. All events that pass the criteria (13) are considered for two γJ-observables:

- the distribution of the rapidity difference $\mathrm{d}(\Delta)\sigma/\mathrm{d}\Delta\eta$, $0 < \Delta\eta < 2.4$, $\Delta\eta = \eta_J - \eta_\gamma$;
- the distribution of the invariant mass of the γJ-pair $\mathrm{d}(\Delta)\sigma/\mathrm{d}M_{\gamma J}$, $M_{\gamma J} < 100$ GeV, $M_{\gamma J}^2 = (p_\gamma + p_J)^2$.

B. Comparison of the EG methods

For the comparison of the EG methods we unfortunately had to restrict ourselves again to the set GRSV $g_{\max}$. The mandatory test of the implementation of the MAW did not yield any surprise. The asymmetries calculated from Born-cross sections with both methods agreed within the relative statistical accuracy of a few per cent.

Before discussing the full results including parton showers we should be careful to check if Frixione's isolation method also works for the string fragmentation model used in Pythia. Hadronization is not an exactly collinear process here, so that some fragmentation photons might actually fulfill the isolation criterion. This is indeed the case, but only for very few events so that we do not need to worry about them and can safely keep fragmentation switched off. Unlike for NLO QCD calculations, where all perturbatively produced photons originate directly in the hard interaction, we need to make a further distinction for perturbatively produced photons in the EG model. Aside from 'direct' photons, which are produced in the LO hard processes $qg \to q\gamma$ and $q\bar{q} \to g\gamma$, there is also the possibility that the photon is produced by emission from a quark line in the PS 'before' or 'after' one of the purely strong interacting reactions $qq \to qq$, $qg \to qg$, $gg \to gg$, etc. occurs. We denote this second source of photons as 'bremsstrahlung' photons. Depending on their transverse momentum they make up 20-40% of all isolated photons at $\sqrt{S} = 200$ GeV according to Fig. 7. The simulation of the bremsstrahlung contribution is very tedious because under normal circumstances only every thousandth event contains an isolated photon. This very low efficiency can be somewhat improved by multiplying the value of α by a small factor (e.g. 3) so that the ratio of QED- to QCD-emissions becomes larger without changing the event characteristics. But even then huge numbers of events are needed for decent statistical accuracies, especially when using Sphinx. We therefore only present the comparison of 'direct' photons in Fig. 8, for which we produced $1.7 \cdot 10^8$ events. We proceed along the same lines as for the jet studies in the last section. At first, the correct treatment of particle helicity in the ISS of Sphinx is switched on resulting in the dashed crosses in the right column. Then the ISS is operated in unpolarized mode resulting in the dotted crosses for R_A. The overall picture is very similar to Fig. 2 but less pronounced. Especially the $p_{T,\gamma}$- and $\Delta\eta$-dependent asymmetries show relative deviations of up to 10% which are again due to the missing treatment of particle helicity in the ISS within the MAW. Keeping in mind that we do not know if the inclusion of bremsstrahlung photons would change the overall picture, we can state that the usage of the MAW for prompt photon simulations *appears* to be better justified than for jet physics. We generated an additional $2.8 \cdot 10^8$ events to study the bremsstrahlung contribution but unfortunately the insufficient statistical accuracy did not allow us to draw any conclusions.

C. Comparison of the MAW with NLO QCD predictions

Before we proceed to the comparison with NLO QCD we should again try to establish a common basis for both methods by checking the Born-level results. Our tests showed that cross sections and asymmetries calculated with the MAW and the parton generator agreed on a 1% level so that everything is in perfect order. This is a strong indication for the correctness of our explanation for the deviations seen in Fig. 3 because colour interference does not exist in LO prompt photon production (see also Table I).

In Fig. 9 the full EG results, i.e. including PS and including QED-bremsstrahlung, are compared with the NLO QCD predictions. Please note, that an overall K-factor of $K = 1.5$ has been applied to all cross sections calculated with the MAW to bring its rates better in line with the NLO predictions. Of course this correction is far from being ideal but it can be justified by the large scale dependence of the EG results. Indeed, it is common practice to more or less trust the shape of cross sections predicted by an EG and to adjust the normalization within certain limits. A slightly larger $K = 1.67$ would have led to a very good agreement for $\mathrm{d}\sigma/\mathrm{d}\Delta\eta$ and $\mathrm{d}\sigma/\mathrm{d}M_{\gamma J}$ but for the price of larger

discrepancies between the inclusive cross sections whose slopes are already way off. With the exception of the critical set DSS3, the asymmetries surprisingly deviate only by 5-10% on average! Due to the small gluon parameterization of DSS3, resulting in the small asymmetries of Fig. 9, the quark-gluon fusion process does not dominate as strongly and other processes become increasingly relevant. The situation becomes a lot more complicated with the effect that the discrepancies between asymmetries reach up to 25%. Unfortunately, the very long computation times prohibited any attempt to improve the agreement by repeating the fit of the shower parameters discussed in section II.

This leaves us with the study of the scale dependence of the NLO predictions presented in Fig. 10. It turns out to be much larger than for jet production so that the different bands of asymmetries partly overlap. With the exception of two bins even the sizable deviations of DSS3 are within the limits. The asymmetries for the two GRSV parameterizations are located near the center of the corresponding bands. At least in this restricted sense, the asymmetries calculated with the MAW and NLO QCD are consistent with each other.

IV. RESUME

Our detailed comparisons between SPHINX and the method of asymmetry weights show, that the correct description of particle polarization in the initial state shower generally has to be implemented into any polarized event generator if one requires a precision of order 10%. For some of the studied observables we find even differences as large as 20% between the MAW and SPHINX. The most drastic deviations arise for the region of large pseudorapidity ($\eta \approx 2$) of 1-jet inclusive observables. Luckily this region of phase-space will be irrelevant for the experiments at RHIC. The geometrical coverage of STAR only reaches out to $\eta = 2$ so that under normal circumstances the maximal pseudorapidity for the jet-axis will be $\eta \approx 1$. So we are left with maximal deviations of approximately 10%, which are however still substantial. In view of the tremendous advantage in speed of the method of asymmetry weights we therefore recommend the following compromise: in a first step, all studies should be performed using the method of asymmetry weights. Once the optimal energies, experimental cuts, etc. have been found, SPHINX should be used to check the results.

The comparisons between event generator and NLO QCD predictions are encouraging despite of the substantial discrepancies in the unpolarized sector. The longitudinal double spin asymmetries are the objects we are mainly interested in and the agreement is much better here. With very few exceptions, the deviations between the method of asymmetry weights and NLO QCD are smaller than the uncertainties of the NLO QCD predictions due to scale dependence. Both methods yield consistent results in this restricted sense. During the starting phase of the RHIC spin project these theoretical uncertainties on the asymmetries of approximately 10% are probably tolerable. However, in the long run more precise event generators will be needed. Their development can in our opinion not be achieved without substantial conceptual progress in event generator techniques. Most likely a fusion of NLO matrix elements with the parton shower methods is needed. The development of such a NLO EG has been a hot topic of scientific debate [18] for several years already due to its urgency. So far, no working solution is available. In view of the substantial costs of the RHIC spin program and the scientific importance of a polarized NLO event generator it would seem advisable to us to also invest the necessary manpower and funds into the development of such a code, which, however, does not seem to happen. Thus, we might soon be in the situation that wonderfully rich data is available but cannot be appropriately analyzed.

ACKNOWLEDGMENTS

This work was supported by the BMBF and the "Deutsche Forschungsgemeinschaft". We thank the authors of Refs. [10,12] for making their parton generator codes available to us. O. Martin is grateful to N. Saito for the invitation to the RIKEN-BNL research center workshop "Event Generator for Spin Physics" and thanks A. Kirchner, L. Niedermeier, S. Schäfer, E. Stein and M. Stratmann for lively discussions during our weekly meetings.

---

[1] O. Martin, A. Schäfer, M. Stratmann and W. Vogelsang, Phys. Rev. **D60**, 117502 (1999).

[2] T. Sjöstrand, Phys. Lett. **B157**, 321 (1985); M. Bengtsson and T. Sjöstrand, Nucl. Phys. **B289**, 810 (1987).

[3] RHIC Spin Collaboration, D. Hill et al., letter of intent RHIC-SPIN-LOI-1991, updated 1993; G. Bunce et al., Particle World **3**, 1 (1992); PHENIX/Spin Collaboration, K. Imai et al., BNL-PROPOSAL-R5-ADD (1994).

[4] R.L. Jaffe and N. Saito, Phys. Lett. **B382**, 165 (1996).

[5] T. Sjöstrand, Comp. Phys. Comm. **82**, 74 (1994).

[6] T. Sjöstrand, PYTHIA *5.7 and* JETSET *7.4 Physics and Manual*, LU TP 95 20, revised version of CERN-TH.7112/93, `hep-ph/9508391`.

[7] S. Güllenstern, P. Gornicki, L. Mankiewicz and A. Schäfer, Comp. Phys. Commun. **87**, 16 (1995); `http://www.physik.uni-regensburg.de/`$\sim$ `mao24852/sphinx.html`.

[8] S. Güllenstern, P. Gornicki, L. Mankiewicz and A. Schäfer, Phys. Rev. **D51**, 3305 (1995).

[9] H.L. Lai et al., Eur. Phys. J.**C12**, 375 (2000).

[10] D. de Florian, S. Frixione, A. Signer and W. Vogelsang, Nucl. Phys. **B539**, 455 (1999).

[11] P. Aurenche, M. Fontannaz, J.Ph. Guillet, B. Kniehl, E. Pilon and M. Werlen, `hep-ph/9811382`.Eur.Phys.J. C9 (1999) 107-119

[12] S. Frixione, `hep-ph/9809397`, in: Proceedings of ICHEP98, XXIX International Conference on High Energy Physics, Vancouver, 23 - 29 July, 1998. S. Frixione and W. Vogelsang, Nucl. Phys. **B**, (2000).Nucl.Phys.B568:60-92,2000

[13] M. Glück, E. Reya and A. Vogt, Z. Phys. **C67**, 433 (1995).

[14] M. Glück, E. Reya, M. Stratmann and W. Vogelsang, Phys. Rev. **D53**, 4775 (1996).

[15] D. de Florian, O.A. Sampayo and R. Sassot, Phys. Rev. **D57**, 5801 (1998).

[16] S. Ellis and D.E. Soper, Phys. Rev. **D48**, 3160 (1993).

[17] S. Frixione, Phys. Lett. **B429**, 369 (1998).

[18] C. Friberg, T. Sjöstrand, `hep-ph/9906316`; J.C. Collins, `hep-ph/0001040`, and references therein.

FIGURE CAPTIONS

Fig. 1 The ratio $K_{(\Delta)g}(x,\mu^2)$ defined in Eq. (8) for the unpolarized and polarized parton densities of our analysis in the relevant x-range. The line style coding of this figure will be used throughout the paper.

Fig. 2 Comparison of jet production calculated with the MAW and SPHINX: (un)polarized cross sections and asymmetries calculated with GRSV $g_{\max}$ and their relative deviations $R_{\sigma,A}$ defined in Eq. (11). Left and center columns: full lines represent the MAW results, dashed lines represent the SPHINX results. Right column: full lines represent R_σ, dashed (dotted) crosses represent R_A calculated with (without) polarized treatment in the ISS of SPHINX.

Fig. 3 The relative deviations $R_{\sigma/A}$ defined in Eq. (12) for the Born results calculated with the MAW and the parton generator. Line styles are chosen according to Fig. 1. The figure is based on $2 \cdot 10^7$ generated events.

Fig. 4 Comparison of jet production calculated with NLO QCD and the MAW with switched-on PS and standard PS parameters. Left column: MAW (NLO QCD) results are represented by full (dashed) lines. Center column: the line styles are chosen according to Fig. 1 with one line representing the NLO QCD and the other one the MAW result for each parametrization. They can be identified from the third column, where the line styles are again chosen according to Fig. 1, i.e. full crosses represent R_σ and all other lines represent R_A for the various parameterizations of polarized parton distributions.

Fig. 5 same as Fig. 4 but with tuned PS parameters which were chosen to improve the agreement between both methods (see text).

Fig. 6 Comparison of the optimized EG results (markers) with the bands of NLO QCD results which are obtained, when the scales are varied by a factor of 2 or 1/2, resp. Left column: full lines represent the band of possible unpolarized NLO QCD cross sections, dashed and dotted lines represent the bands of polarized NLO QCD cross sections and follow the same pattern as in Fig. 1. Right column: corresponding minimal and maximal NLO QCD predictions for the asymmetries. Line Styles are again chosen according to Fig. 1. The large scale dependence for 20 GeV$< M_{JJ} <$30 GeV is due to the fact that this bin receives no contribution to $\mathcal{O}(\alpha_s^2)$ so that all values are effectively only LO predictions.

Fig. 7 Relative contribution of 'direct' and 'bremsstrahlung' photons to the total production rate of isolated photons.

Fig. 8 Same as Fig. 2 but for the production of 'direct' photons (without 'bremsstrahlung' contribution).

Fig. 9 Same as Fig. 4 but for the production of isolated photons (including the 'bremsstrahlung contribution'). A K-factor of $K = 1.5$ is applied to all EG cross sections. The figure is based on $3 \cdot 10^8$ generated events.

Fig. 10 Same as Fig. 6 but for the production of isolated photons. A K-factor of $K = 1.5$ is applied to all EG cross sections.

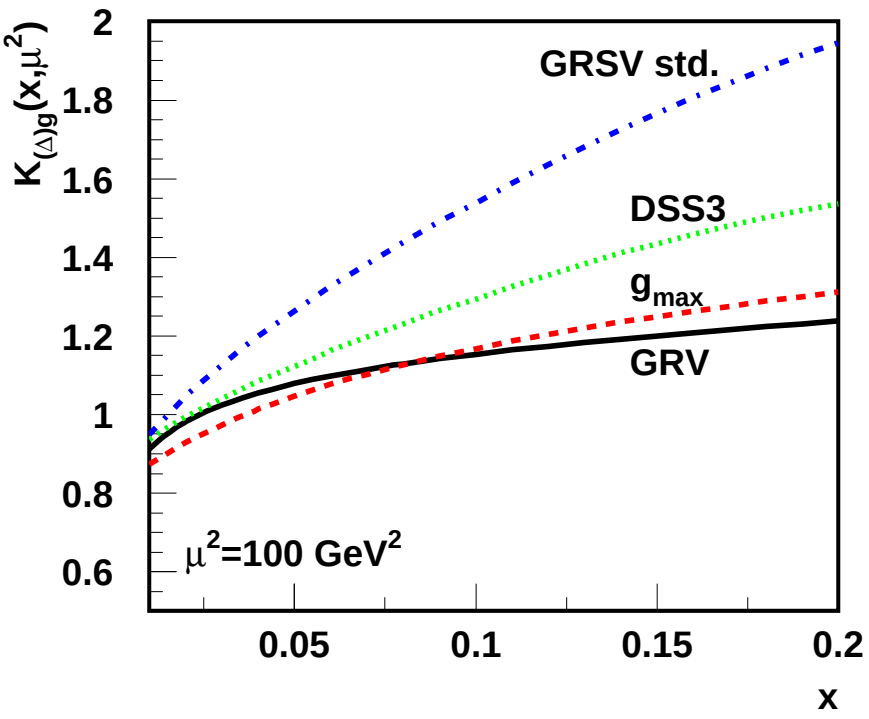
$K_{(\Delta)g}(x,\mu^2)$
2
1.8
1.6
1.4
1.2
1
0.8
0.6
GRSV std.
DSS3
g_{max}
GRV
μ^2=100 GeV^2
0.05
0.1
0.15
0.2
x

FIG. 1.

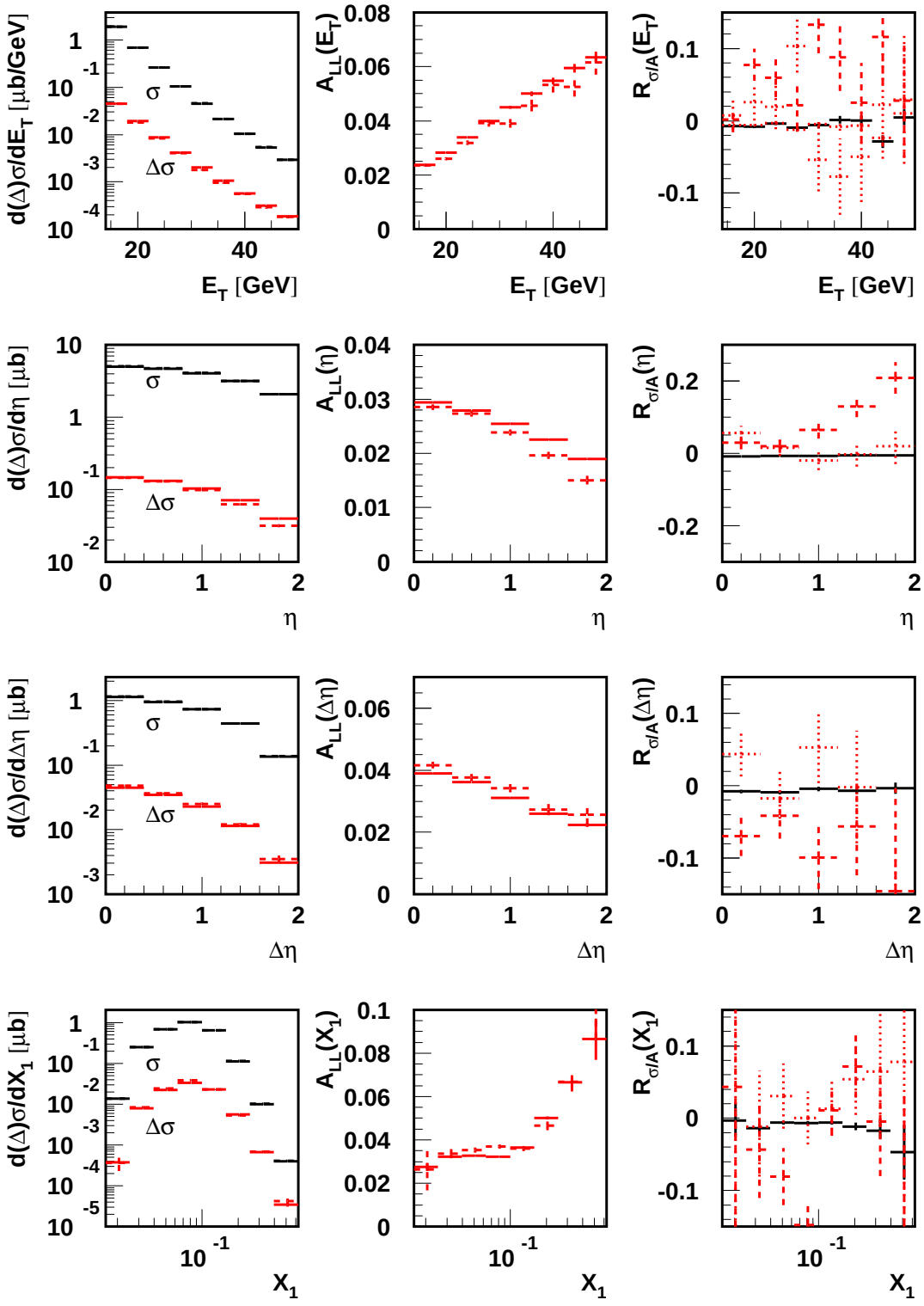
d(Δ)σ/dE_T [μb/GeV]
σ
Δσ
E_T [GeV]
A_LL(E_T)
R_σ/A(E_T)
d(Δ)σ/dη [μb]
η
A_LL(η)
R_σ/A(η)
d(Δ)σ/dΔη [μb]
Δη
A_LL(Δη)
R_σ/A(Δη)
d(Δ)σ/dX_1 [μb]
X_1
A_LL(X_1)
R_σ/A(X_1)

FIG. 2.

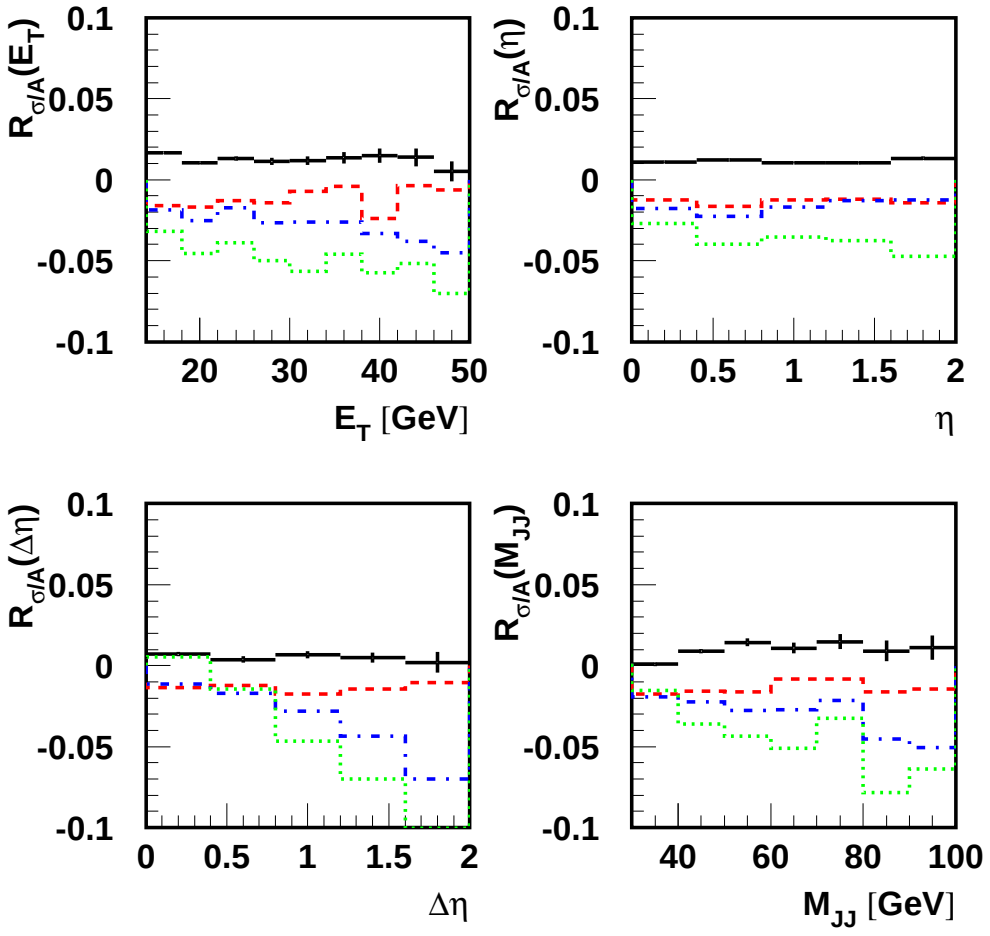
$R_{\sigma/A}(E_T)$
E_T [GeV]
$R_{\sigma/A}(\eta)$
η
$R_{\sigma/A}(\Delta\eta)$
$\Delta\eta$
$R_{\sigma/A}(M_{JJ})$
M_{JJ} [GeV]

FIG. 3.

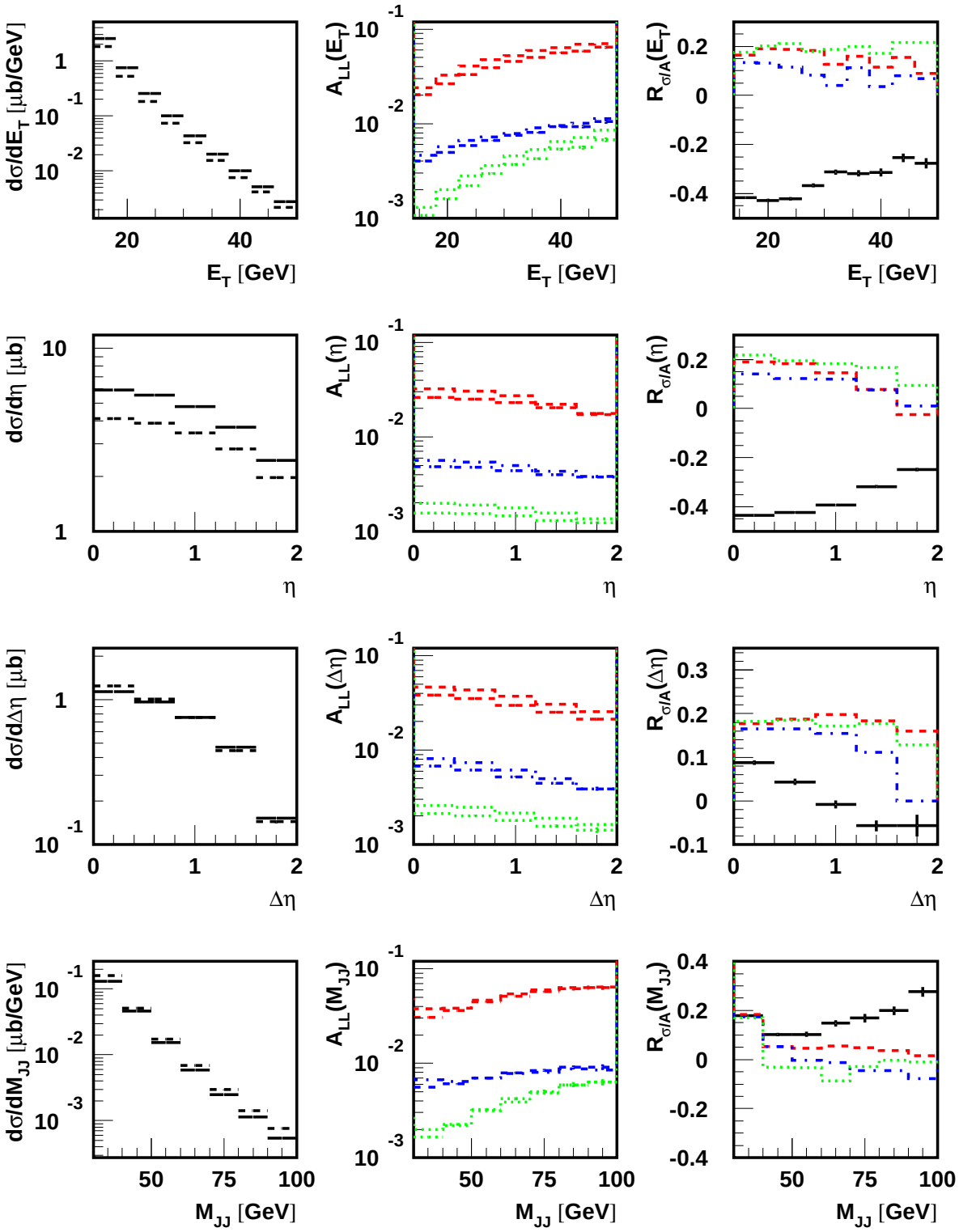
dσ/dE_T [μb/GeV]
E_T [GeV]
A_LL(E_T)
R_σ/A(E_T)
dσ/dη [μb]
η
A_LL(η)
R_σ/A(η)
dσ/dΔη [μb]
Δη
A_LL(Δη)
R_σ/A(Δη)
dσ/dM_JJ [μb/GeV]
M_JJ [GeV]
A_LL(M_JJ)
R_σ/A(M_JJ)

FIG. 4.

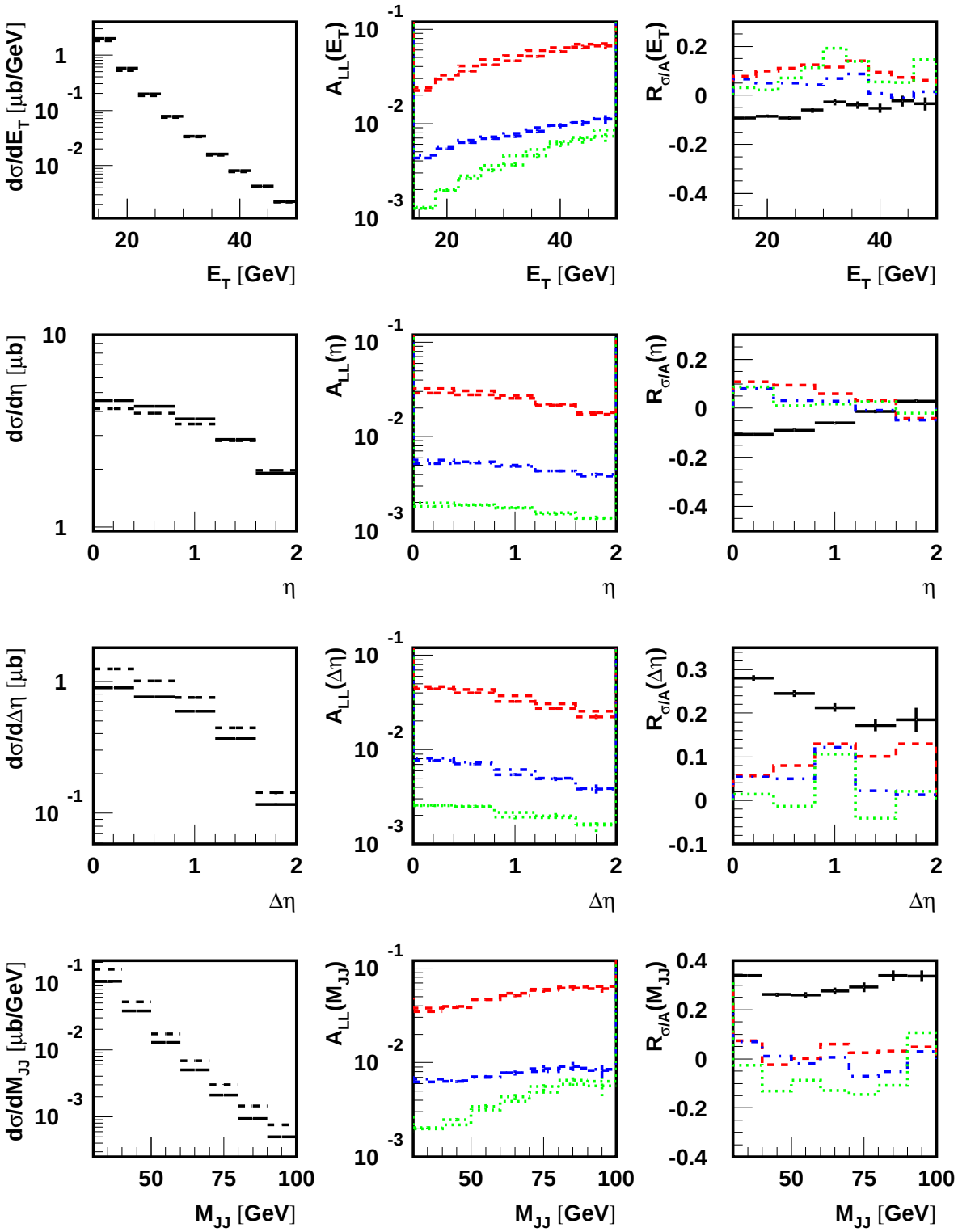
dσ/dE_T [μb/GeV]
E_T [GeV]
A_LL(E_T)
R_σ/A(E_T)
dσ/dη [μb]
η
A_LL(η)
R_σ/A(η)
dσ/dΔη [μb]
Δη
A_LL(Δη)
R_σ/A(Δη)
dσ/dM_JJ [μb/GeV]
M_JJ [GeV]
A_LL(M_JJ)
R_σ/A(M_JJ)

FIG. 5.

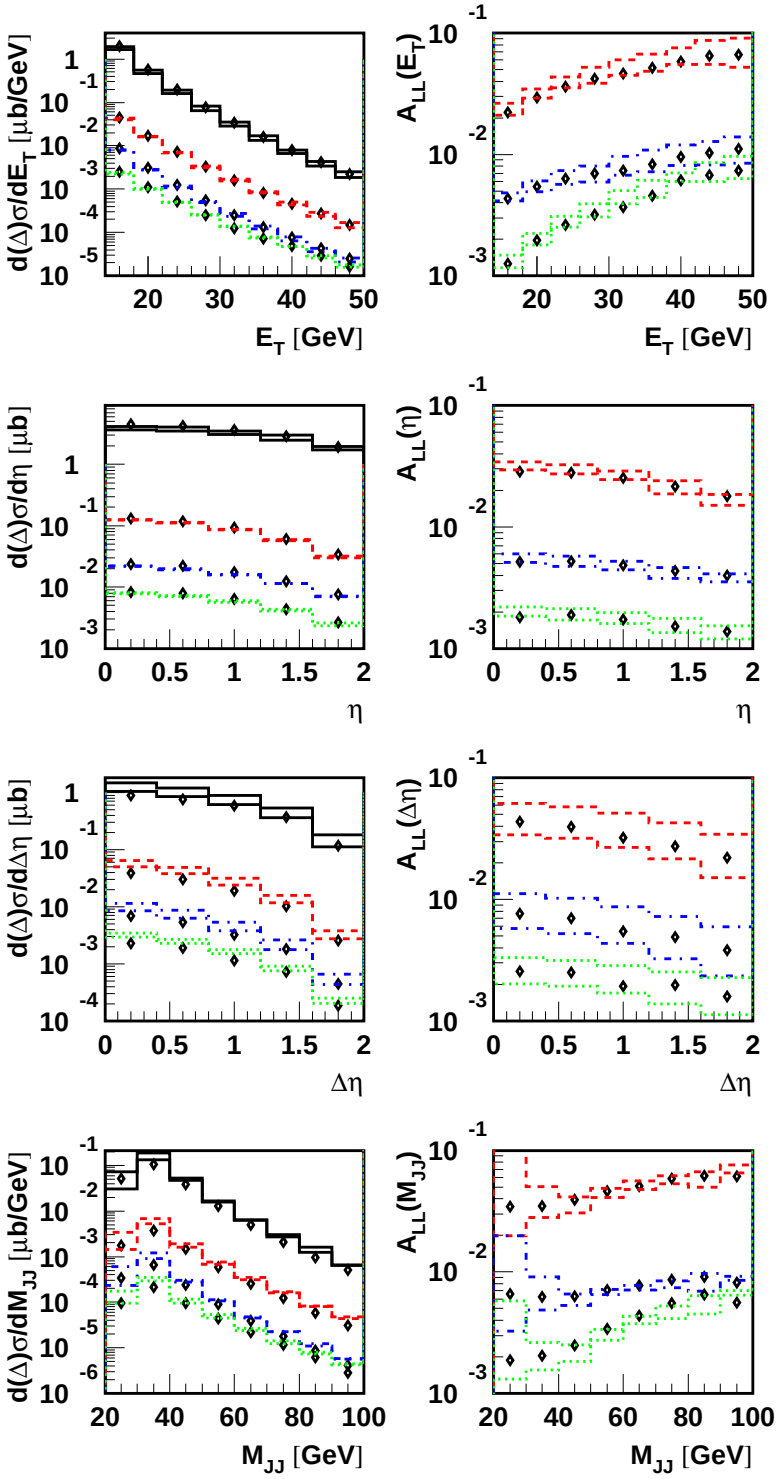
d(Δ)σ/dE_T [μb/GeV]
E_T [GeV]
A_LL(E_T)
E_T [GeV]
d(Δ)σ/dη [μb]
η
A_LL(η)
η
d(Δ)σ/dΔη [μb]
Δη
A_LL(Δη)
Δη
d(Δ)σ/dM_JJ [μb/GeV]
M_JJ [GeV]
A_LL(M_JJ)
M_JJ [GeV]

FIG. 6.

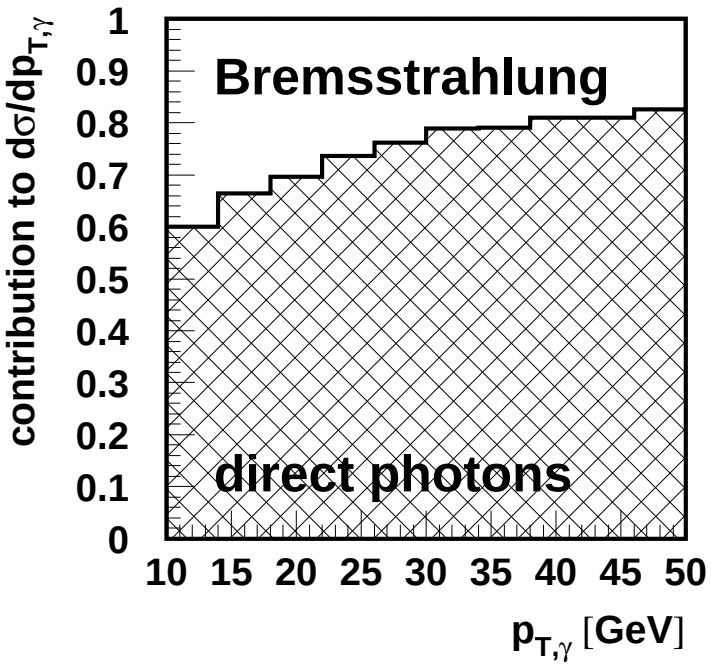
Bremsstrahlung
direct photons
contribution to dσ/dp$_{T,\gamma}$
p$_{T,\gamma}$ [GeV]
0
0.1
0.2
0.3
0.4
0.5
0.6
0.7
0.8
0.9
1
10
15
20
25
30
35
40
45
50

FIG. 7.

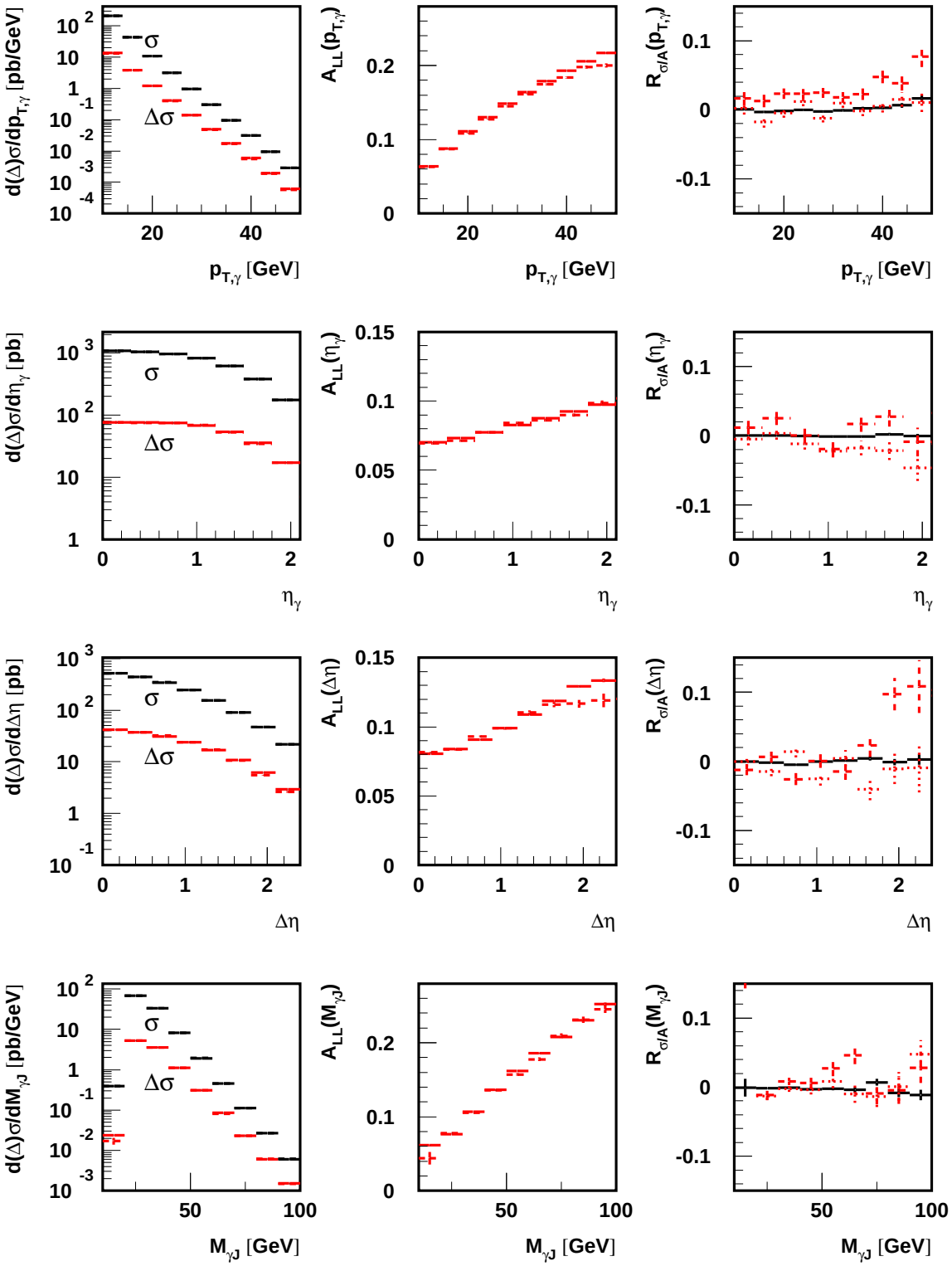
d(Δ)σ/dp_{T,γ} [pb/GeV]
σ
Δσ
A_LL(p_{T,γ})
R_{σ/A}(p_{T,γ})
p_{T,γ} [GeV]
d(Δ)σ/dη_γ [pb]
A_LL(η_γ)
R_{σ/A}(η_γ)
η_γ
d(Δ)σ/dΔη [pb]
A_LL(Δη)
R_{σ/A}(Δη)
Δη
d(Δ)σ/dM_{γJ} [pb/GeV]
A_LL(M_{γJ})
R_{σ/A}(M_{γJ})
M_{γJ} [GeV]

FIG. 8.

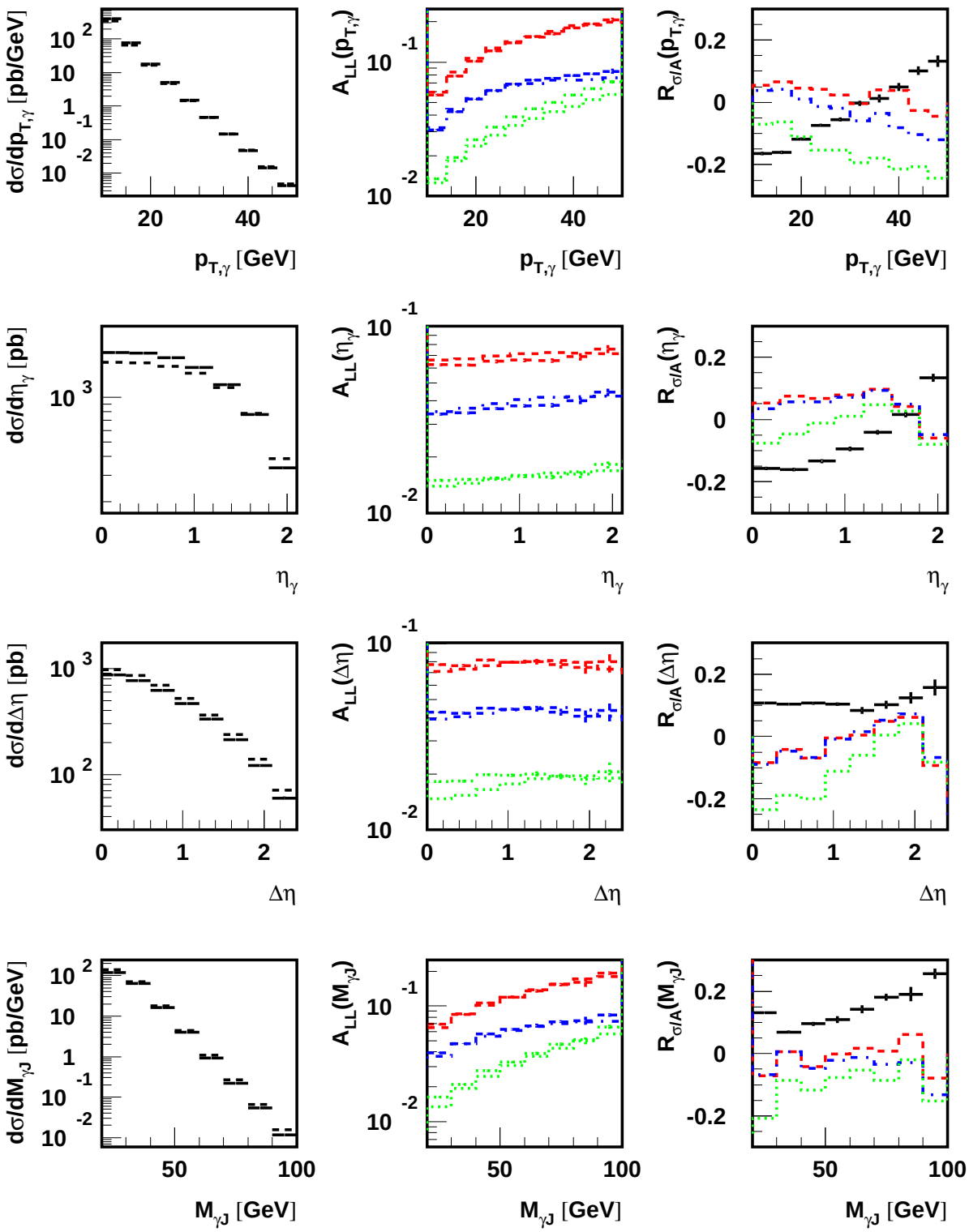
dσ/dp_{T,γ} [pb/GeV]
A_LL(p_{T,γ})
R_{σ/A}(p_{T,γ})
p_{T,γ} [GeV]
dσ/dη_γ [pb]
A_LL(η_γ)
R_{σ/A}(η_γ)
η_γ
dσ/dΔη [pb]
A_LL(Δη)
R_{σ/A}(Δη)
Δη
dσ/dM_{γJ} [pb/GeV]
A_LL(M_{γJ})
R_{σ/A}(M_{γJ})
M_{γJ} [GeV]

FIG. 9.

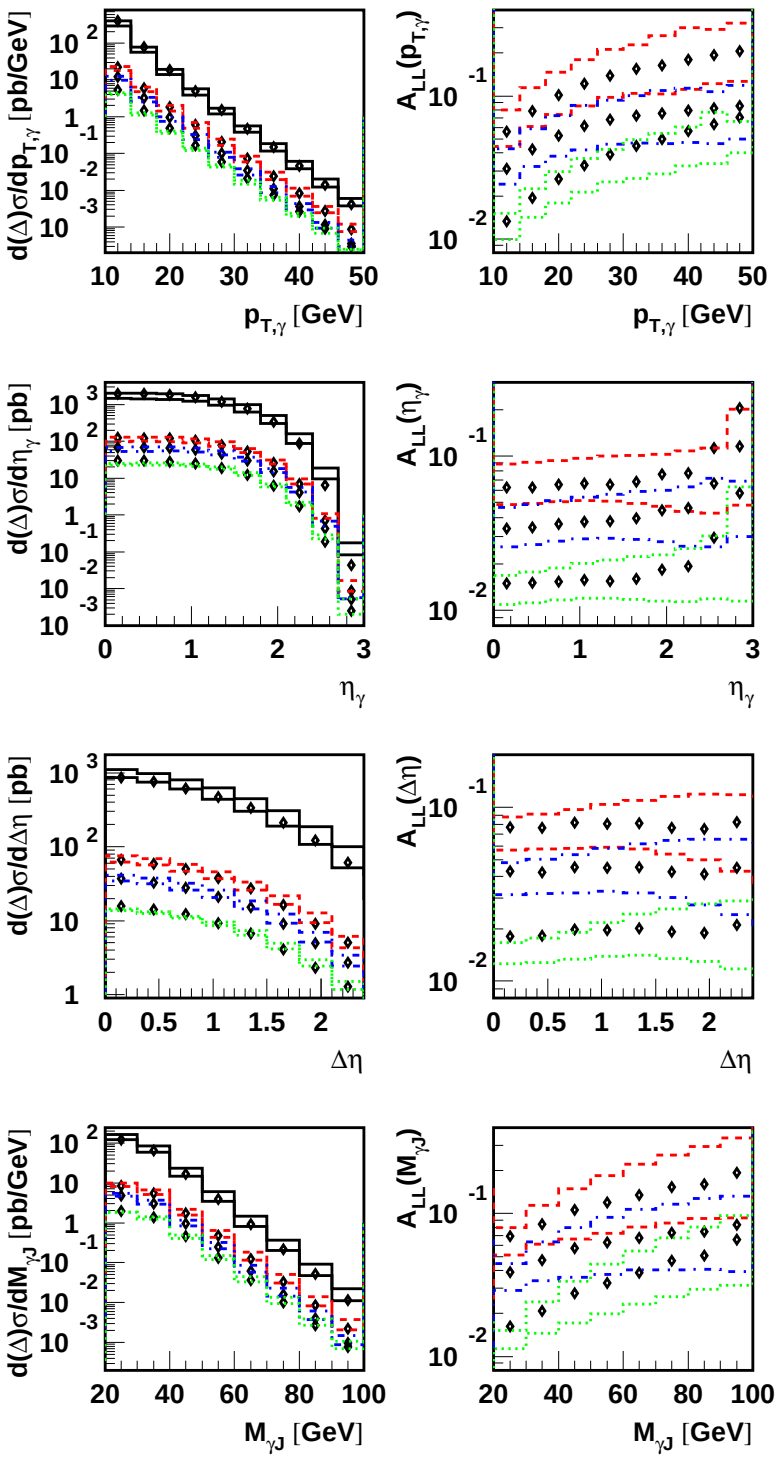
d(Δ)σ/dp_{T,γ} [pb/GeV]
A_LL(p_{T,γ})
p_{T,γ} [GeV]
d(Δ)σ/dη_γ [pb]
A_LL(η_γ)
η_γ
d(Δ)σ/dΔη [pb]
A_LL(Δη)
Δη
d(Δ)σ/dM_{γJ} [pb/GeV]
A_LL(M_{γJ})
M_{γJ} [GeV]

FIG. 10.